Relativistic Density Functional Study of the Geometry, Electronic Transitions, Ionization Energies, and Vibrational Frequencies of Protactinocene, Pa(η^8-C_8H_8)$_2$

Jun Li and Bruce E. Bursten*

Contribution from the Department of Chemistry, The Ohio State University, Columbus, Ohio 43210

Received June 18, 1998. Revised Manuscript Received September 9, 1998

Abstract: The geometric structure and electronic properties of the $5f^1$ complex protactinocene, Pa(COT)$_2$ (COT = η^8-C_8H_8), have been investigated using gradient-corrected density functional methods with the inclusion of spin−orbit coupling. The calculated structure of Pa(COT)$_2$ with scalar relativistic corrections is intermediate between those of Th(COT)$_2$ and U(COT)$_2$. Spin−orbit effects are essential for the calculation of state energies of Pa(COT)$_2$. Under D_{8h}* double-group symmetry, the ground state is found to be an $E_{5/2u}$ state that corresponds to an $(f\phi)^1$ electron configuration. The first excited state ($E_{1/2u}$) lies only about 0.05 eV above the ground state. The low-lying states follow the ordering of $E_{5/2u}$ ($f\phi$) < $E_{1/2u}$ ($f\sigma+f\pi$) ≪ $E_{3/2u}$ ($f\pi$) ∼ $E_{7/2u}$ ($f\phi$) < $2E_{1/2u}$ ($f\pi+f\sigma$) < $E_{1/2g}$ ($d\sigma$) ≪ $2E_{3/2u}$ ($f\delta$) < $2E_{5/2u}$ ($f\delta$). The lowest-energy electric-dipole-allowed f → d electronic transition is calculated to occur at 368 nm, which is in excellent agreement with the experimental estimation of 365 nm. The first 20 vertical ionization energies and the magnetic moment of Pa(COT)$_2$ have been predicted as based on the spin−orbit calculations. A comparison of the calculated infrared vibrational frequencies and absorption intensities of Pa(COT)$_2$ with the available experimental data is presented, and the vibrational spectra are assigned.

Introduction

The theoretical prediction[1] and subsequent experimental discovery[2] of the actinide sandwich complex uranocene, U(COT)$_2$ (COT = η^8-C_8H_8), was a milestone in the organometallic chemistry of actinides. This chemistry has since expanded to include the synthesis of a wide variety of other actinocenes, An(COT)$_2$ (An = Th, Pa, Np, Pu, Am), and actinocene anions.[3] Several theoretical methods have been used to elucidate the electronic structures, bonding, and electronic spectra of various actinocenes and lanthanocenes.[4−8]

The actinide atom in a neutral actinocene is in the formal +4 oxidation state. As a consequence, protactinocene, Pa(COT)$_2$, is an f^1 complex and should provide the most direct data about the influence of the (COT)$_2$ ligand field on a 5f electron. Indeed, at the end of his classic review paper on the ligand field theory of f-orbital sandwich complexes, Warren proposed that "high upon the list of desirable experimental information must however be a study of the magnetic and electronic spectral properties of the $5f^1$ complex, Pa(COT)$_2$, ESR investigation of f^1 and f^3 systems, measurement of anisotropic susceptibilities, and further spectral and MCD studies of all the actinocenes." [9] However, because of the small quantities of protactinium available and its pronounced radioactivity, the chemistry of protactinium compounds is still largely undeveloped, thus hampering a systematic comparison across the early actinide series. Although more than two decades have passed since Warren's review, the available data on protactinocene are scant; only X-ray powder diffraction data and some vibrational and visible spectra have been experimentally reported for protactinocene or its analogue with 1,3,5,7-$C_8H_4Me_4$ (TMCOT) ligands.[10,11]

Because of the experimental difficulties inherent in the study of Pa(COT)$_2$, high-quality theoretical methods can play a particularly important role in elucidating the electronic properties of this unique compound. The f^1 electron configuration and high symmetry of the protactinocene simplify the theoretical interpretation of its bonding, electronic spectral properties, and magnetic data, thus providing the opportunity to carry out benchmarking theoretical studies. Prior calculations of the electronic structure of protactinocene were performed by using

(1) Fischer, R. D. *Theor. Chim. Acta (Berlin)* **1963**, *1*, 418.
(2) Streitwieser, A., Jr.; Müller-Westerhoff, U. *J. Am. Chem. Soc*. **1968**, *90*, 7364.
(3) (a) Streitwieser, A., Jr.; Kinsley, S. A. *NATO ASI Ser. C* **1985**, *155*, 77 and references therein. (b) Streitwieser, A., Jr. *Inorg. Chim. Acta* **1984**, *94*, 171.
(4) (a) Pyykkö, P. *Inorg. Chim. Acta* **1987**, *139*, 243. (b) Pepper, M.; Bursten, B. E. *Chem. Rev.* **1991**, *91*, 719. (c) Balasubramanian, K. In *Handbook on the Physics and Chemistry of Rare Earths*; Gschneidner, K. A., Jr., Eyring, L., Eds.; Elsevier: Amsterdam, 1994; Vol. 18, p 29. (d) Dolg, M.; Stoll, H. In *Handbook on the Physics and Chemistry of Rare Earths*; Gschneidner, K. A., Jr., Eyring, L., Eds.; Elsevier: Amsterdam, 1996; Vol. 22, p 607.
(5) (a) Rösch, N.; Streitwieser, A., Jr. *J. Am. Chem. Soc*. **1983**, *105*, 7237. (b) Rösch, N. *Inorg. Chim. Acta* **1984**, *94*, 297. (c) Dolg, M.; Fulde, P.; Küchle, W.; Neumann, C.-S.; Stoll, H. *J. Chem. Phys*. **1991**, *94*, 3011. (d) King, R. B. *Inorg. Chem*. **1992**, *31*, 1978. (e) Cory, M. G.; Köstlmeier, S.; Kotzian, M.; Rösch, N.; Zerner, M. C. *J. Chem. Phys*. **1994**, *100*, 1353. (f) Dolg, M.; Fulde, P.; Stoll, H.; Preuss, H.; Chang, A. H. H.; Pitzer, R. M. *Chem. Phys*. **1995**, *195*, 71. (g) Liu, W.; Dolg, M.; Fulde, P. *J. Chem. Phys.* **1997**, *107*, 3584. (h) Liu, W.; Dolg, M.; Fulde, P. *Inorg. Chem.* **1998**, *37*, 1067. (i) Dolg, M.; Fulde, P. *Eur. J. Chem.* **1998**, *4*, 200.
(6) Chang, A. H. H.; Zhao, K.; Ermler, W. C.; Pitzer, R. M. *J. Alloys Compd.* **1994**, *213/214*, 191.
(7) Boerrigter, P. M.; Baerends, E. J.; Snijders, J. G. *Chem. Phys.* **1988**, *122*, 357.
(8) Chang, A. H. H.; Pitzer, R. M. *J. Am. Chem. Soc.* **1989**, *111*, 2500.
(9) Warren, K. D. *Struct. Bond.* **1977**, *33*, 97.
(10) (a) Starks, D. F.; Parsons, T. C.; Streitwieser, A., Jr.; Edelstein, N. *Inorg. Chem*. **1974**, *13*, 1307. (b) Goffart, J.; Fuger, J.; Brown, D.; Duyckaerts, G. *Inorg. Nucl. Chem. Lett*. **1974**, *10*, 413.
(11) Solar, J. P.; Burghard, H. P. G.; Banks, R. H.; Streitwieser, A., Jr.; Brown, D. *Inorg. Chem*. **1980**, *19*, 2186.

10.1021/ja9821145 CCC: $15.00
Published on Web 10/22/1998

relativistic extended Hückel,[12] DV-Xα,[13] Hartree−Fock−Slater (HFS),[7] and spin−orbit configuration interaction (SOCI) methods.[6,14] The HFS calculations by Boerrigter et al. were the first systematic density functional study of the actinocenes.[7] Although this excellent study surveyed the bonding and electronic ground states in actinocenes, the electronic transitions of protactinocene were not considered. Further, because the experimental geometry of $Pa(COT)_2$ was unknown and theoretical optimization of the geometry was not possible, these previous calculations were based on nonoptimized geometries.

In this contribution, we will report the geometric and electronic structure of $Pa(COT)_2$ as calculated by relativistic density functional theory (DFT) with the utilization of gradient-corrected exchange-correlation functionals. Excited-state calculations have been carried out with the explicit inclusion of relativistic spin−orbit effects, which are very significant in heavy-element complexes.[4,15] These DFT studies provide the first calculations of the optimized structure and vibrational properties of $Pa(COT)_2$ and will also provide direct comparisons to previous calculations of its optical transition energies by the DV-Xα[13] and SOCI[6,14] methods.

Computational Details

All calculations were carried out using the Amsterdam Density Functional (ADF) code Version 2.3 (Theoretical Chemistry, Vrije Universiteit, Amsterdam, The Netherlands), developed by Baerends et al.,[16] which incorporates the relativistic extensions first proposed by Snijders et al.[17] The code was vectorized by Ravenek,[18] and the numerical integration scheme applied for the calculations was developed by te Velde et al.[19] The frozen core approximation has been applied to the inner orbitals, i.e., [1s] for C and [1s−5d] for Pa. The STO valence basis sets used for C and H are double-ζ plus 3d-type polarization function (DZP), and the valence basis sets for the protactinium are triple-ζ (TZ).[20]

To evaluate the effect of different density functionals on the geometry and transition energy, the geometry optimization and state energy calculations employed a variety of exchange and correlation functionals, from the HFS and local density approach (LDA),[21] to the gradient-corrected methods using exchange-correlation functionals of Becke−Lee−Yang−Parr (BLYP), Becke−Perdew (BP86), and Perdew−Wang (PW91).[22] Most of the calculations were accomplished with the PW91 method, which is known to be one of the best generalized gradient approaches. The scalar relativistic effects were taken into account during the geometry optimizations by use of the quasi-relativistic method.[23] The relativistic spin−orbit (SO) effects have been included through double-group calculations based on the geometries determined in the scalar relativistic optimization.

The geometry of $Pa(COT)_2$ has been fully optimized under restriction of D_{8h} symmetry using the analytical energy gradient method implemented in ADF 2.3. Electronic transition energies were calculated as the difference in total energy between excited states and the ground state, whereas the ionization energies are determined by Slater's transition-state method.[24]

Table 1. Optimized Geometries for $Pa(COT)_2$ with Different DFT Functionals

	HFS	LDA	BLYP	BP86	PW91	expt av[a]
Pa−X[b] (Å)	1.937	1.915	2.040	1.984	1.975	1.964 ± 0.010
Pa−C (Å)	2.667	2.650	2.755	2.711	2.702	2.674 ± 0.004
C−C (Å)	1.404	1.402	1.417	1.413	1.412	1.389 ± 0.013
C−H (Å)	1.100	1.097	1.092	1.093	1.092	1.090
∠XCH (deg)	173.8	174.3	171.4	172.7	172.7	

[a] The listed experimental values are averages of the corresponding crystallographic parameters of $Th(COT)_2$ and $U(COT)_2$ (ref 27). [b] X is the centroid of the COT ring.

Results and Discussion

Geometry. The theoretical determination of metal−ring distances in sandwich compounds is a significant challenge in electronic structure calculations on transition metal complexes, such as ferrocene,[25] and in actinide complexes.[5,26] The protactinocene molecule is generally assumed to have the same D_{8h} structure as the other actinocenes. Our PW91-optimized structures of the eclipsed (D_{8h}) and staggered (D_{8d}) conformers of $Pa(COT)_2$ indicate that the energy difference between the two conformers is less than 0.1 kcal/mol. Thus, the $Pa(COT)_2$ molecule is expected to exhibit free rotation of the two COT rings relative to one another. We will therefore consider only the D_{8h} structure in this paper.

Table 1 lists the Pa−X (X = COT centroid), Pa−C, C−C, and C−H distances and ∠HCX angles optimized using the HFS, LDA, BLYP, BP86, and PW91 density functionals. Although the experimental geometry of $Pa(COT)_2$ is unavailable for comparison, the Pa−X distance optimized by the gradient-corrected methods, except BLYP, lies between the experimental An−X distances of $Th(COT)_2$ (2.004 Å) and $U(COT)_2$ (1.923 Å),[27] which augurs well for the validity of these gradient-corrected density functional methods. The Pa−X distances from the HFS and the LDA are, as is typical, too short. By using the average geometric parameters of $Th(COT)_2$ and $U(COT)_2$ as a gauge, the PW91 exchange-correlation functional seems to be the best choice for this system, while BLYP and BP86 generate slightly longer bond distances. The PW91-optimized geometry under D_{8h} symmetry is presented in Figure 1. In

(12) Pyykkö, P.; Laaksonen, L. J.; Tatsumi, K. *Inorg. Chem.* **1989**, *28*, 1801.
(13) Kaltsoyannis, N.; Bursten, B. E. *J. Organomet. Chem.* **1997**, *528*, 19.
(14) Zhao, K. Ph.D. Dissertation, The Ohio State University, Columbus, Ohio, 1996.
(15) See, for example: (a) Kaltsoyannis, N. *J. Chem. Soc., Dalton Trans.* **1997**, 1. (b) Pyykkö, P. *Chem. Rev.* **1988**, *88*, 563. (c) Desclaux, J. P. *Phys. Scr.* **1980**, *21*, 436.
(16) (a) Baerends, E. J.; Ellis, D. E.; Ros, P. *Chem. Phys.* **1973**, *2*, 42. (b) Baerends, E. J.; Ros, P. *Chem. Phys.* **1973**, *2*, 51. (c) Baerends, E. J.; Ros, P. *Int. J. Quantum Chem.* **1978**, *S12*, 169.
(17) (a) Snijders, J. G.; Baerends, E. J. *J. Mol. Phys.* **1978**, *36*, 1789. (b) Snijders, J. G.; Baerends, E. J.; Ros, P. *Mol. Phys.* **1979**, *38*, 1909.
(18) Ravenek, W. In *Algorithms and Applications on Vector and Parallel Computes*; te Riele, H. J. J., DeDekker, Th. J., van de Vorst, H. A., Eds.; Elsevier: Amsterdam, 1987.
(19) (a) Boerrigter, P. M.; te Velde, G.; Baerends, E. J. *Int. J. Quantum Chem.* **1988**, *33*, 87. (b) te Velde, G.; Baerends, E. J. *J. Comput. Phys.* **1992**, *99*, 94.
(20) (a) Snijders, J. G.; Baerends, E. J.; Vernooijs, P. *At. Nucl. Data Tables* **1982**, *26*, 483. (b) Vernooijs, P.; Snijders, J. G.; Baerends, E. J. *Slater Type Basis Functions for the Whole Periodic System*; Internal Report, Free University of Amsterdam, The Netherlands, 1984.
(21) (a) The HFS method uses Slater's Xα (α = 0.7) pure-exchange electron-gas formulation with no correlation functional. (b) LDA exchange functional: see, for example, Ziegler, T. *Chem. Rev.* **1991**, *91*, 651. (c) LDA correlation functional: Vosko, S. H.; Wilk, L.; Nusair, M. *Can. J. Phys.* **1980**, *58*, 1200.
(22) (a) BLYP exchange functional: Becke, A. D. *Phys. Rev. A* **1988**, *38*, 3098. (b) BLYP correlation functional: Lee, C.; Yang, W.; Parr, R. G. *Phys. Rev. B* **1988**, *37*, 785. (c) BP86 correlation functional: Perdew, J. P. *Phys. Rev. B* **1986**, *33*, 8822; **1986**, *34*, 7406 (erratum). (d) PW91 functional: Perdew, J. P.; Wang, Y. *Phys. Rev.* **1992**, *B45*, 13244.
(23) Ziegler, T.; Baerends, E. J.; Snijders, J. G.; Ravenek, W. *J. Phys. Chem.* **1989**, *93*, 3050.
(24) Slater, J. C. *Adv. Quantum Chem.* **1972**, *6*, 1.
(25) (a) Koch, H.; Jørgensen, P.; Helgaker, T. *J. Chem. Phys.* **1996**, *104*, 9528. (b) Pierloot, K.; Persson, B. J.; Roos, B. O. *J. Phys. Chem.* **1995**, *99*, 3465. (c) Park, C.; Almlöf, J. *J. Chem. Phys.* **1991**, *95*, 1829. (d) Lüthi, H. P.; Siegbahn, P. E. M.; Almlöf, J.; Fægri, K., Jr..; Heiberg, A. *Chem. Phys. Lett.* **1984**, *111*, 1. (e) Taylor, T. E.; Hall, M. B. *Chem. Phys. Lett.* **1985**, *114*, 338.
(26) See, for example: Li, J.; Bursten, B. E. *J. Am. Chem. Soc.* **1997**, *119*, 9021.
(27) Avdeef, A.; Raymond, K. N.; Hodgson, K. O.; Zalkin, A. *Inorg. Chem.* **1972**, *11*, 1083.

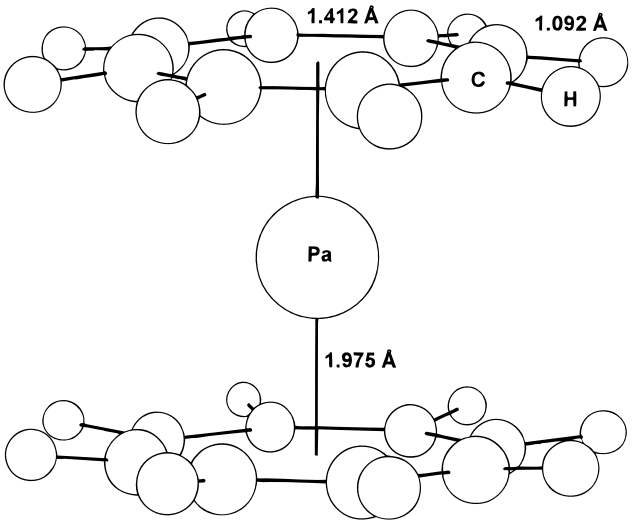

Figure 1. Ball-and-stick representation of the optimized PW91 geometry of $Pa(COT)_2$ under the constraint of D_{8h} symmetry.

agreement with previous theoretical prediction,[28] the H atoms on the C_8H_8 ring are found to be tilted inward (toward the Pa atom) by 6−9°. This calculated nonplanarity of the COT rings may call into question the assumption of planar COT rings that has been made in previous calculations on $Pa(COT)_2$.

In our experience, the scalar relativistic effects dominate the effects of relativity on the geometries of actinide complexes; our benchmark calculations on similar organoactinide complexes indicate that the inclusion of spin−orbit effects has minimal effects on the calculated bond distances or angles.[29] Therefore, no effort has been made to optimize the geometry of $Pa(COT)_2$ with spin−orbit effects included.

Electronic States and Spin−Orbit Effects. Since the ground-state electronic structure of the $Pa(COT)_2$ has been previously discussed in detail,[7,13,14] we will only briefly summarize here some results that will facilitate our subsequent discussion. The eight C 2pπ orbitals of a planar D_{8h} C_8H_8 ligand form eight π molecular orbitals, which, in order of increasing energy, are bases for the a_{2u}, e_{1g}, e_{2u}, e_{3g}, and b_{1u} representations.[26] We will denote the π MOs as π_0, π_1, π_2, π_3, and π_4. In a D_{8h} $M(COT)_2$ complex, these π MOs form gerade π_{ng} and ungerade π_{nu} ($n = 0-4$) group orbitals of $(C_8H_8)_2$. The symmetry matches of these ligand group orbitals with the Pa valence orbitals are listed in Table 2. Without spin−orbit coupling, the 6d orbitals are split in a D_{8h} field as a_{1g} (dσ) ≪ e_{2g} (dδ) < e_{1g} (dπ); the dδ and dπ orbitals are considerably destabilized by strong interaction with the ligand orbitals. Similarly, the Pa 5f orbitals are split as e_{3u} (fϕ) ∼ a_{2u} (fσ) < e_{1u} (fπ) ≪ e_{2u} (fδ), where the strong destabilization of the fδ orbitals from the f-manifold is an indication of their strong interaction with the filled π_{2u} orbitals of the COT ligands. Because of the pseudoaxial symmetry of the D_{8h} ligand field, the splitting of the d and f orbitals preserves $|m_l|$ as a good quantum number, with σ, π, δ, and ϕ corresponding to $m_l = 0$, ±1, ±2, and ±3, respectively. As is typically the case in organoactinide complexes,[30] the splitting of the 6d orbitals is much greater than that of the 5f orbitals because the former have a more diffuse radial distribution. A qualitative molecular orbital diagram for $Pa(COT)_2$ under D_{8h} symmetry is presented in Figure 2.

Table 2. Correlation of the Symmetry Species of the D_{8h} Single Group and the D_{8h}* Double Group

Γ_i (D_{8h})	Pa basis	$(COT)_2$ basis	$\Gamma_i \times e_{1/2g}$ (D_{8h}*)
a_{1g}	s, dσ	π_{0g}	$e_{1/2g}$
a_{2g}			$e_{1/2g}$
b_{1g}		π_{4g}	$e_{7/2g}$
b_{2g}			$e_{7/2g}$
e_{1g}	dπ	π_{1g}	$e_{1/2g} + e_{3/2g}$
e_{2g}	dδ	π_{2g}	$e_{3/2g} + e_{5/2g}$
e_{3g}		π_{3g}	$e_{5/2g} + e_{7/2g}$
a_{1u}			$e_{1/2u}$
a_{2u}	pσ, fσ	π_{0u}	$e_{1/2u}$
b_{1u}			$e_{7/2u}$
b_{2u}		π_{4u}	$e_{7/2u}$
e_{1u}	pπ, fπ	π_{1u}	$e_{1/2u} + e_{3/2u}$
e_{2u}	fδ	π_{2u}	$e_{3/2u} + e_{5/2u}$
e_{3u}	fϕ	π_{3u}	$e_{5/2u} + e_{7/2u}$

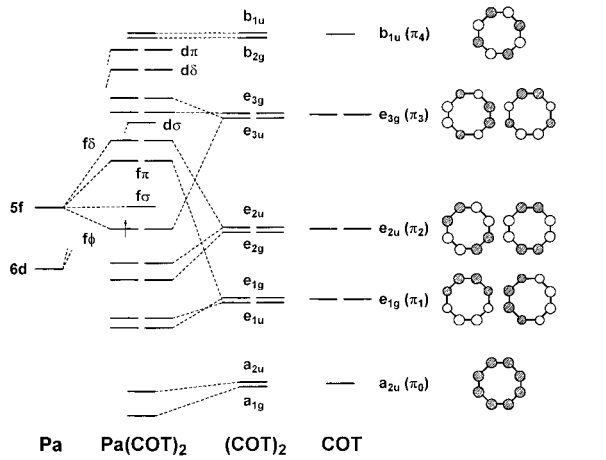

Figure 2. Qualitative molecular orbital diagram for $Pa(COT)_2$ under the D_{8h} single group, showing the principal interactions of the Pa 6d and 5f orbitals with the π orbitals of the two COT rings.

The Pa fσ and fϕ orbitals are low-lying and comparable in energy, largely because these 5f orbitals interact only minimally with the ligand orbitals. Consideration of only the π interactions between the Pa atom and the COT ligands would lead to the prediction that the fϕ orbitals are the lowest in the 5f manifold of $Pa(COT)_2$, as shown in Figure 2. By contrast, our DFT calculations in the absence of spin−orbit coupling predict that the ground state of $Pa(COT)_2$ is the $^2A_{2u}$ state that corresponds to an $(f\sigma)^1$ outer configuration; i.e., the combination of all metal−ligand interactions serves to destabilize the fϕ orbital slightly more than the fσ. The near degeneracy of the fσ and fϕ orbitals suggests that the nature of the ground state will be strongly dependent on spin−orbit effects.

The effects of spin−orbit coupling on an f^1 ion is well developed.[31] The f orbitals are split into a low-lying 6-fold degenerate level with $j = 5/2$ and a higher-lying 8-fold degenerate level with $j = 7/2$. After the coupling of **l** and **s**, m_l and m_s are no longer good quantum numbers. Rather, the f orbitals are indexed by their j and m_j quantum numbers as $|jm_j\rangle$ eigenstates. Table 3 presents the Clebsch−Gordan vector coupling coefficients[32] that express the free-ion $|j,\pm m_j\rangle$ spin−orbit eigenstates with the $|l,\pm m_l\rangle$ eigenstates, i.e., the fσ, fπ, fδ, and fϕ orbitals. These Clebsch−Gordan coefficients will

(28) Elian, M.; Chen, M. M. L.; Mingos, M. P.; Hoffmann, R. *Inorg. Chem.* **1976**, *15*, 1148.

(29) Li, J.; Bursten, B. E. Unpublished results.

(30) Bursten, B. E.; Strittmatter, R. J. *Angew. Chem.* **1991**, *103*, 1085; *Angew. Chem., Int. Ed. Engl.* **1991**, *30*, 1069.

(31) For a discussion of spin−orbit coupling of f electrons, see, for example: Abragam, A.; Bleaney, B. *Electron Paramagnetic Resonance of Transition Ions*; Clarendon Press: Oxford, 1970.

(32) Slater, J. C. *Quantum Theory of Atomic Structure, Vol. II*; McGraw-Hill: New York, 1960.

Table 3. Expansions of the $|jm_j\rangle$ Eigenstates in Terms of Clebsch−Gordan Coefficients for the fσ ($m_l = 0$), fπ ($m_l = \pm1$), fδ ($m_l = \pm2$), and fϕ ($m_l = \pm3$) Orbitals and Spin Functions (α or β)

$\|jm_j\rangle$	expansion	$\|jm_j\rangle$	expansion
$\|5/2,+1/2\rangle$	$-\sqrt{3/7}f_0\alpha + \sqrt{4/7}f_{+1}\beta$	$\|5/2,-1/2\rangle$	$\sqrt{3/7}f_0\beta - \sqrt{4/7}f_{-1}\alpha$
$\|5/2,+3/2\rangle$	$-\sqrt{2/7}f_{+1}\alpha + \sqrt{5/7}f_{+2}\beta$	$\|5/2,-3/2\rangle$	$\sqrt{2/7}f_{-1}\beta - \sqrt{5/7}f_{-2}\alpha$
$\|5/2,+5/2\rangle$	$-\sqrt{1/7}f_{+2}\alpha + \sqrt{6/7}f_{+3}\beta$	$\|5/2,-5/2\rangle$	$\sqrt{1/7}f_{-2}\beta - \sqrt{6/7}f_{-3}\alpha$
$\|7/2,+1/2\rangle$	$\sqrt{4/7}f_0\alpha + \sqrt{3/7}f_{+1}\beta$	$\|7/2,-1/2\rangle$	$\sqrt{4/7}f_0\beta + \sqrt{3/7}f_{-1}\alpha$
$\|7/2,+3/2\rangle$	$\sqrt{5/7}f_{+1}\alpha + \sqrt{2/7}f_{+2}\beta$	$\|7/2,-3/2\rangle$	$\sqrt{5/7}f_{-1}\beta + \sqrt{2/7}f_{-2}\alpha$
$\|7/2,+5/2\rangle$	$\sqrt{6/7}f_{+2}\alpha + \sqrt{1/7}f_{+3}\beta$	$\|7/2,-5/2\rangle$	$\sqrt{6/7}f_{-2}\beta + \sqrt{1/7}f_{-3}\alpha$
$\|7/2,+7/2\rangle$	$f_{+3}\alpha$	$\|7/2,-7/2\rangle$	$f_{-3}\beta$

allow us to analyze the relative effects of spin−orbit coupling and the ligand field on the intermediate coupling states of Pa(COT)$_2$.[33]

We will now combine the splitting of the f orbitals under a D_{8h} field with the spin−orbit splitting of an f^1 ion. The electronic structure of Pa(COT)$_2$ with the inclusion of spin−orbit coupling requires that the molecule be treated under the D_{8h}* double group.[34] The correlation of the irreducible representations of the D_{8h} single group and the D_{8h}* double group can be derived by taking the direct product of the single-group representations with the one-electron spin representation ($e_{1/2g}$), as listed in Table 2. Because of the half-integer spin angular momentum ($s = {}^1/_2$), all the doubly degenerate spatial orbitals, which are 4-fold spin degenerate under the single group, are split into two doubly degenerate spin−orbitals (spinors); these Kramers doublets[35] result from the degeneracy of orbitals with the same value of $|m_j|$.[31] The splitting of the $|jm_j\rangle$ eigenstates when the spherical symmetry is lowered to D_{8h}* is

$$j = 5/2: \quad e_{1/2u} + e_{3/2u} + e_{5/2u}$$

$$j = 7/2: \quad e_{1/2u} + e_{3/2u} + e_{5/2u} + e_{7/2u}$$

Figure 3 shows the correlation between the ligand-field and spin−orbit splitting in Pa(COT)$_2$, leading to the spinors under D_{8h}* symmetry in the center column. As we have seen for other f^1 actinide complexes, the ultimate splitting pattern of the 5f-based orbitals is a compromise between the splitting of the 5f orbitals by spin−orbit coupling and the splitting induced by the ligand field.[36] Spin−orbit coupling leads to considerable splitting of the predominantly 5f-based degenerate single-group MOs of Pa(COT)$_2$, namely the $3e_{3u}$ (81% fϕ), $5e_{1u}$ (92% fπ), and $4e_{2u}$ (80% fδ) orbitals. Among the ligand-based orbitals, the $4e_{3u}$ and $4e_{2g}$ MOs, which have significant contributions from the Pa 5f and 6d orbitals, respectively, experience large splitting as well. Figure 4 shows the correlation of the low-lying Pa-based orbitals of Pa(COT)$_2$, from the scalar-relativistic atomic orbitals of a Pa atom, to the spin−orbitals of the molecule, labeled under the D_{8h}* point group.

Because Pa in Pa(COT)$_2$ has an f^1 configuration with only one unpaired electron, the states that result from various configurations will have the same symmetry as the orbital in which the unpaired electron resides. At the PW91-optimized geometry, the calculated PW91 ground state of Pa(COT)$_2$ is the $E_{5/2u}$ state that arises from the $(e_{5/2u})^1$ configuration. This $E_{5/2u}$ state is derived predominantly from the $^2E_{3u}$ L−S state,

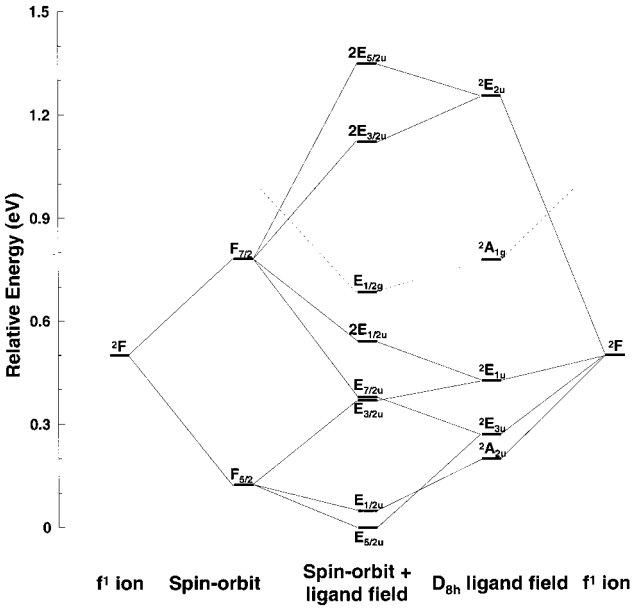

Figure 3. Correlation diagram showing the combined effects of the ligand field and spin−orbit coupling on the state energies of Pa(COT)$_2$. The two left columns show the splitting of the ^2F term due to spin−orbit coupling, and the right two columns show the splitting of the ^2F term under a D_{8h} ligand field such as provided by two COT ligands. The central column shows the intermediate coupling case under the D_{8h}* double group in which both spin−orbit and ligand-field effects are significant. The states connected with a dashed line are due to the excited d^1 electron configuration.

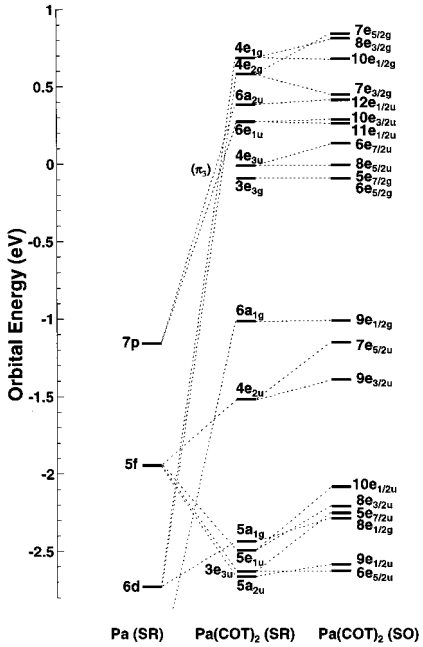

Figure 4. Correlation of the orbitals of Pa and Pa(COT)$_2$ with the inclusion of scalar-relativistic (SR) corrections under D_{8h} symmetry and of spin−orbit (SO) corrections under D_{8h}* symmetry.

which corresponds to the $(f\phi)^1$ configuration. Although the $^2E_{2u}$ state of the $(f\delta)^1$ configuration could, by symmetry, contribute to the $E_{5/2u}$ ground state, the high energy of the $(f\delta)^1$ configuration makes it a negligible contributor to the ground state. An analysis of the $|jm_j\rangle$ eigenstate contributions to the ground state is also consistent with this description. The ground state is nearly entirely derived from the $|5/2,\pm5/2\rangle$ free-ion eigenstate, with only a 6% contribution from the $|7/2,\pm5/2\rangle$ eigenstate. The

(33) For a discussion of intermediate coupling, see, for example: Gerloch, M. *Orbitals, Terms and States*; John Wiley & Sons: Chichester, 1986.

(34) An extensive compilation of all the point groups can be found in, for example: Altmann, S. L.; Herzig, P. *Point-Group Theory Tables*; Clarendon Press: Oxford, 1994.

(35) Kramers, H. A. *Proc. Acad. Sci. Amst.* **1930**, *33*, 959.

(36) See, for example: Kaltsoyannis, N.; Bursten, B. E. *Inorg. Chem.* **1995**, *34*, 2735.

Table 4. Comparison of LDA, BLYP, PW91, and SOCI State Energies (eV) for Some Low-Lying States of $Pa(COT)_2$

state	configuration	LDA	BLYP	PW91	PW(TS)[a]	PW(Nopt)[b]	SOCI[c]	ΔE
$E_{5/2u}$	e_{3u} (f^1)	0.000	0.000	0.000	0.000	0.000	0.000	0.000
$E_{1/2u}$	$a_{2u} + e_{1u}$ (f^1)	0.131	−0.036	0.049	0.041	0.101	0.166	0.065
$E_{3/2u}$	e_{1u} (f^1)	0.460	0.274	0.369	0.375	0.395	0.477	0.082
$E_{7/2u}$	e_{3u} (f^1)	0.354	0.408	0.379	0.378	0.362	0.362	0.000
$2E_{1/2u}$	$e_{1u} + a_{2u}$ (f^1)	0.601	0.472	0.541	0.523	0.567	0.569	0.002
$E_{1/2g}$	a_{1g} (d^1)	0.633	0.735	0.685	0.598	0.651	0.925	0.274
$2E_{3/2u}$	e_{2u} (f^1)	1.307	0.953	1.122	1.141	1.227	1.222	−0.005
$2E_{5/2u}$	e_{2u} (f^1)	1.545	1.171	1.350	1.383	1.463	1.427	−0.036
$3E_{5/2u}$	$(e_{2u})^3(e_{3u})^2$ (π^3f^2)	2.916	2.838	2.896	2.956	2.873		
$3E_{3/2u}$	$(e_{2u})^3(e_{3u})^2$ (π^3f^2)	2.946	2.865	2.924	2.982	2.901		

[a] The PW(TS) calculations employ the PW91 functional and use the transition-state method for excited-state energies. [b] The PW(Nopt) energies are PW91 energies calculated at the geometry assumed in the SOCI calculations. [c] The spin−orbit CI results are taken from ref 14.

Clebsch−Gordan coefficients in Table 3 indicate that the $|5/2,\pm5/2\rangle$ eigenstate is derived predominantly from the fϕ orbitals. Therefore, the ground state can be described as primarily derived from the $(f\phi)^1$ configuration.

The first excited state, an $E_{1/2u}$ state, is calculated to lie only ca. 400 cm^{-1} above the ground state, which is only slightly higher than the kT value (207 cm^{-1}) at ambient temperature. This $E_{1/2u}$ state is a nearly pure $|5/2,\pm1/2\rangle$ eigenstate, with only 1% contribution from $|7/2,\pm1/2\rangle$. The fact that this state is a nearly pure $|jm_j\rangle$ eigenstate is in accord with the strong mixing of the $(f\sigma)^1$ (41%) and $(f\pi)^1$ (55%) configurations (Table 3), consistent with the relative energetic proximity of the $^2A_{2u}$ and $^2E_{1u}$ single-group states. The second and the third excited states are calculated to be quite close to each other in energy. The second excited state is an $E_{3/2u}$ state, which can be described as a strong mixture of the fπ (43%) and fδ (50%) orbitals. This state exhibits strong mixing between the $|5/2,\pm3/2\rangle$ (55%) and $|7/2,\pm3/2\rangle$ (38%) free-ion eigenstates. This mixing between $|jm_j\rangle$ and $|j+1,m_j\rangle$ states is quite common in the ground state of some actinide compounds and usually results in significant effects on the ground-state magnetic properties.[37] The third excited state is an $E_{7/2u}$ state. This state is derived entirely from the $|7/2,\pm7/2\rangle$ eigenstate, which in turn corresponds to a pure $(f\phi)^1$ configuration.

Note that the ordering of the states does not follow the same ordering as the spin−orbitals. For example, consider the $E_{1/2g}$ state, which is derived from the $(d\sigma)^1$ configuration and corresponds to occupation of the relatively low-lying $8e_{1/2g}$ orbital. Despite the low energy of the orbital, the $E_{1/2g}$ state is higher in energy than all of the states that arise from occupation of the fσ, fϕ, and fπ orbitals. This effect is a consequence of differential electron−electron repulsion between different states that is not reflected entirely in the orbital energies.[38]

To compare the calculated state energies from DFT and from spin−orbit CI methods, we list in Table 4 the calculated LDA, BLYP, PW91, and spin−orbit CI state energies for the important low-lying states of $Pa(COT)_2$. In addition to the $E_{5/2u}$ ground state, we also include excited f^1 and $(d\sigma)^1$ states arising from the ^2F and ^2D terms as well as two ligand-to-metal charge transfer (LMCT) states with f^2 configurations. The principal electron configurations in the single-group representations are also included in Table 4 in order to facilitate analysis. The LDA, BLYP, and PW91 state energies in Table 4 are calculated at the geometry optimized for each of these density functionals. The state energies labeled PW(TS) are calculated using the PW91 method with Slater's transition state (TS) method,[24] and those labeled PW(Nopt) use the nonoptimized geometry that was used in the SOCI calculation.[14]

It is evident from Table 4 that the state energies calculated by the LDA and PW91 methods are quite comparable to those of the more expensive spin−orbit CI calculations. The consistency of the LDA results might be somewhat fortuitous considering its much shorter calculated Pa−COT distance. The results using the BLYP functional are also comparable to the others, with the major deviation being that the $E_{1/2u}$ state is predicted to be the ground state. This difference is likely related to the longer optimized Pa−COT distance obtained from this method. Note that the PW91 and BLYP calculations with the optimized geometries predict that the $E_{7/2u}$ state is slightly higher in energy than the $E_{3/2u}$, whereas the LDA and SOCI calculations predict the opposite. This discrepancy is likely the result of the too-short Pa−COT distance employed in the LDA and SOCI calculations. In fact, the PW(Nopt) calculations, which use the same geometry as used in the SOCI calculation [i.e. the crystallographic experimental geometry of $U(COT)_2$], predict the same ordering of state energies as the SOCI calculation. The relative energies calculated by the PW(Nopt) and SOCI methods are in excellent agreement, with the exception of the d^1 $E_{1/2g}$ state. The reason for this discrepancy is unclear, and no experimental value is available for comparison. We note, however, that the SOCI energies calculated for the f → d excited states of uranocene are ca. 45% too high compared to the experimental ones,[8] while the SOCI energy for protactinocene is 42% higher than our PW91 energy for the f → d energy difference. Inasmuch as these high-lying diffuse d-states require a more flexible basis set, we suspect that this difference could be attributed to the smaller d-orbital basis set (double-ζ) used in the SOCI calculation.[39] This comparison suggests that the gradient-corrected DFT methods, especially PW91, can be used as a reliable theoretical method for large actinide molecules where a spin−orbit CI calculation is too expensive to be carried out.

It is worth noting that the energy difference determined by using the transition-state method including spin−orbit effects is within ±0.08 eV of that calculated by the state energy difference, thereby confirming the applicability of the former method to heavy-element systems when spin−orbit effects are included. Table 4 also shows that the states from the f^2 configurations are much higher in energy than those from the f^1 configurations or $(d\sigma)^1$ configuration. Therefore, protactinocene is, indeed, best described as an f^1 compound.

Electronic Transitions. The electronic spectra in actinide compounds usually involve a combination of f → f, f → d, and

(37) Lam, D. J.; Chan, S. K. *Phys. Rev. B* **1972**, *6*, 307.

(38) Thornton, G; Edelstein, N.; Rösch, N. *J. Chem. Phys.* **1979**, *70*, 5218.

(39) We have undertaken benchmark PW91 calculations with a much more extended basis set (triple-ζ functions on all atoms, with d and f polarization functions on C, and p and d polarization functions on H). The calculated state energies match those in Table 4 very closely; e.g. the $E_{1/2g}$ state is still 0.245 eV closer to the ground state than it is in the SOCI calculations.

Table 5. PW91 Excitation Energies for the Transitions from the $6e_{5/2u}$ Orbital to Excited Orbitals of $Pa(COT)_2$[a]

excited orbital	excited state	transition type	ΔE (cm^{-1})	ΔE (nm)	polarization[b]
$9e_{1/2u}$	$E_{1/2u}$	f → f	393	25459	
$8e_{1/2g}$	$E_{1/2\,g}$	f → d	5528	1809	
$5e_{7/2u}$	$E_{7/2u}$	f → f	3059	3269	
$8e_{3/2u}$	$E_{3/2u}$	f → f	2978	3358	
$10e_{1/2u}$	$E_{1/2u}$	f → f	4364	2291	
$9e_{3/2u}$	$E_{3/2u}$	f → f	9049	1105	
$7e_{5/2u}$	$E_{5/2u}$	f → f	10890	918	
$9e_{1/2g}$	$E_{1/2g}$	f → s	18567	539	
$6e_{5/2g}$	$E_{5/2g}$	f → π_3	25158	397	*z*
$5e_{7/2g}$	$E_{7/2g}$	f → π_3	25162	397	(*x*,*y*)
$8e_{5/2u}$	$E_{5/2u}$	f → π_3	24027	416	
$6e_{7/2u}$	$E_{7/2u}$	f → π_3	24660	406	
$11e_{1/2u}$	$E_{1/2u}$		29278	342	
$10e_{3/2u}$	$E_{3/2u}$		29573	338	
$12e_{1/2u}$	$E_{1/2u}$		29421	340	
$7e_{3/2g}$	$E_{3/2g}$	f → d	27166	368	(*x*,*y*)
$10e_{1/2g}$	$E_{1/2g}$	f → d	30071	333	
$8e_{3/2g}$	$E_{3/2g}$	f → d	31427	318	(*x*,*y*)
$7e_{5/2g}$	$E_{5/2g}$	f → d	30664	326	*z*
$9e_{3/2g}$	$E_{3/2g}$		41763	239	(*x*,*y*)
$8e_{5/2g}$	$E_{5/2g}$		42059	238	*z*
$11e_{1/2g}$	$E_{1/2g}$		43375	231	
$6e_{7/2g}$	$E_{7/2g}$	f → π_4	46075	217	(*x*,*y*)
$10e_{3/2g}$	$E_{3/2g}$		44673	224	(*x*,*y*)

[a] Transitions are listed in the order of the spin-orbital energies. [b] Transitions with no polarization listed are electric-dipole-forbidden.

charge-transfer transitions. These spectra are generally quite complicated, not only because of the large number of states derived from a single f^n configuration, but also because of the splitting of these states by the ligand-field and spin−orbit coupling. Fortunately, the electronic transitions in protactinocene are relatively straightforward because it is an f^1 complex. The PW91 transition energies for all the excitations from the $6e_{5/2u}$ level to the virtual levels up to $10e_{3/2g}$ are listed in Table 5. The transitions are listed in the order of the virtual orbital energies, which emphasizes the deviations of the excited-state energy ordering from the orbital energy ordering.

Because of the high symmetry and the f^1 configuration of $Pa(COT)_2$, only a small number of the electronic transitions are dipole-allowed. First, because of the centrosymmetry of the molecule, allowed transitions must involve a parity change.[40] More specifically in the D_{8h}* double group, for an electric-dipole-allowed transition from the $E_{5/2u}$ ground state, the excited state has to be one of the $E_{3/2g}$, $E_{5/2g}$, or $E_{7/2g}$ states. As a consequence of these selection rules, all of the f → f transitions, which are predicted to occur in the IR (infrared) or near-IR region, are forbidden because they do not involve a parity change. We include these transitions in our tabulation because of the possibility that they could gain some intensity via vibronic coupling. In addition, although the d-based states have gerade (g) symmetry, all of the $E_{5/2u} \rightarrow nE_{1/2g}$ transitions are still forbidden. Only the f → d and f → π_3 transitions $E_{5/2u} \rightarrow E_{3/2g}$ (*x*,*y* polarization), $E_{5/2u} \rightarrow E_{5/2g}$ (*z* polarization), and $E_{5/2u} \rightarrow E_{7/2g}$ (*x*,*y* polarization) are allowed.

The lowest-energy allowed excitations of the Pa 5f-localized electron in $Pa(COT)_2$ are the $E_{5/2u} \rightarrow E_{5/2g}$ and $E_{5/2u} \rightarrow E_{7/2g}$ transitions, which are both predicted to occur at 397 nm. These excitations promote the Pa 5f electron to the strongly antibonding $3e_{3g}$ (π_3) orbitals of the ligands, which should significantly increase the Pa−COT distance. The lowest-energy allowed f → d transition is predicted to be the $E_{5/2u} \rightarrow E_{3/2g}$ transition, which results from excitation of the electron from the $6e_{5/2u}$ to the $7e_{3/2g}$ spin-orbital. This transition corresponds to an excitation from the $(f\phi)^1$ ground configuration to the $(d\delta)^1$ excited configuration, with slight mixing of the $d\pi$ orbitals. The calculated transition energy, 27 200 cm^{-1} or 368 nm, is in near-perfect agreement with the experimental estimate of 365 nm by Streitwieser and co-workers.[11] The nearly quantitative agreement between the calculated value and the experimental estimate may be somewhat fortuitous; nevertheless, we believe that the closeness of the calculated value is not surprising, given that DFT methods have previously been found to reproduce experimental excitation energies quite well.[41]

In addition to the excitations of the 5f electron discussed above, we have also calculated the energies of LMCT transitions from filled COT orbitals into empty metal-based orbitals. Table 6 lists the calculated transition energies for all the electric-dipole-allowed excitations from the four COT π_2-based orbitals, $5e_{5/2u}$, $7e_{3/2u}$, $5e_{5/2g}$, and $6e_{3/2g}$, to the virtual f, d, and π_3 orbitals between $6e_{5/2u}$ and $10e_{3/2g}$ (see Figure 4). We find only two LMCT transitions that should occur in the visible region (430−435 nm), corresponding to the transitions from $3e_{2u}$-based ligand orbitals ($5e_{5/2u}$ and $7e_{3/2u}$) to the Pa dσ orbital ($8e_{1/2g}$). All other dipole-allowed transitions, including those in Table 5, are predicted to occur in the UV region, suggesting that the protactinocene should have a rich UV spectrum.

The LMCT transitions that promote an electron from the strongly bonding orbitals, e_{2u}-5fδ or e_{2g}-6dδ, to Pa−COT nonbonding or antibonding orbitals will increase the Pa−COT distance in the excited states, thus suggesting strong Franck−Condon effects.[42] A reoptimization of one of the LMCT excited state with the $(3e_{2u})^3(f\phi)^1(d\sigma)^1$ configuration indicates that the Pa−COT distance is lengthened by about 0.02 Å. An exhaustive discussion of the Franck−Condon effects on these LMCT transitions would require reoptimization of the geometries for each state, including spin−orbit interactions. This procedure is not computationally practicable at present. Further, most of the LMCT transitions involve triple open-shells, which create four excited Kramers doublets for each configuration. The energy splitting of these excited states belonging to the same open-shell configuration is usually small, and we have not pursued a further calculation of the multiplets arising from each configuration.

We will conclude our discussion of the electronic transitions of $Pa(COT)_2$ by summarizing our results and comparing them to the available experimental data and to previous theoretical calculations. Our calculations have probed the likely allowed ligand-field (LF), metal-to-ligand charge transfer (MLCT), and LMCT transitions in the molecule. Of these, we find only a small number that are expected to contribute to the optical spectroscopy of protactinocene at wavelengths $\lambda \geq 350$ nm: $\pi_2 \rightarrow$ d LMCT (430, 435 nm; visible), f → π_3 MLCT (397 nm; UV−visible edge), and fϕ → dδ LF (368 nm; near-UV). Unfortunately, there is a paucity of experimental spectra for $Pa(COT)_2$ to which these results can be compared. Protactinocene itself is a golden yellow solid.[10] Although there are no reports of the optical spectrum of $Pa(COT)_2$, the wavelengths of the optical transitions of the octamethyl derivative $Pa(TMCOT)_2$ have been reported as tabular data; neither extinction coefficients nor a reproduction of the actual spectrum was given.

(40) See, for example: Douglas, B. E.; Hollingsworth, C. A. *Symmetry in Bonding and Spectra. An Introduction*; Academic Press: Orlando, 1985.

(41) See, for example: (a) Daul, C.; Baerends, E. J.; Vernooijs, P. *Inorg. Chem.* **1994**, *33*, 3538. (b) Bellafrouh, K.; Daul, C.; Guedel, H. U.; Gilardoni, F.; Weber, J. *Theor. Chim. Acta* **1995**, *91*, 215. (c) Dickson, R. M.; Ziegler, T. *Int. J. Quantum Chem.* **1996**, *58*, 681.

(42) Haken, H.; Wolf, H. C. *Molecular Physics and Elements of Quantum Chemistry*; Springer-Verlag: Berlin, 1995.

Table 6. PW91 Transition Energies for the Electric-Dipole-Allowed Excitations from the π_2-Based Orbitals of $Pa(COT)_2$[a]

transition	type	excited states	ΔE (cm^{-1})	ΔE (nm)
$5e_{5/2u} \rightarrow 8e_{1/2g}$	$\pi_2 \rightarrow d$	$2E_{1/2g} + E_{5/2g} + E_{7/2g}$	22964	435
$5e_{5/2u} \rightarrow 9e_{1/2g}$	$\pi_2 \rightarrow s$	$2E_{1/2g} + E_{5/2g} + E_{7/2g}$	34451	290
$5e_{5/2u} \rightarrow 6e_{5/2g}$	$\pi_2 \rightarrow \pi_3$	$E_{1/2g} + 3E_{5/2g}$	40786	245
$5e_{5/2u} \rightarrow 5e_{7/2g}$	$\pi_2 \rightarrow \pi_3$	$E_{1/2g} + E_{3/2g} + 2E_{7/2g}$	40791	245
$5e_{5/2u} \rightarrow 7e_{3/2g}$	$\pi_2 \rightarrow d$	$3E_{3/2g} + E_{7/2g}$	45591	219
$7e_{3/2u} \rightarrow 8e_{1/2g}$	$\pi_2 \rightarrow d$	$E_{1/2g} + E_{3/2g} + 2E_{7/2g}$	23252	430
$7e_{3/2u} \rightarrow 9e_{1/2g}$	$\pi_2 \rightarrow s$	$E_{1/2g} + E_{3/2g} + 2E_{7/2g}$	34829	287
$7e_{3/2u} \rightarrow 6e_{5/2g}$	$\pi_2 \rightarrow \pi_3$	$3E_{3/2g} + E_{7/2g}$	41171	243
$7e_{3/2u} \rightarrow 5e_{7/2g}$	$\pi_2 \rightarrow \pi_3$	$2E_{1/2g} + E_{5/2g} + E_{7/2g}$	41175	243
$7e_{3/2u} \rightarrow 7e_{3/2g}$	$\pi_2 \rightarrow d$	$E_{1/2g} + 3E_{5/2g}$	45899	218
$5e_{5/2g} \rightarrow 6e_{5/2u}$	$\pi_2 \rightarrow f$	$E_{5/2g}$	29090	344
$5e_{5/2g} \rightarrow 9e_{1/2u}$	$\pi_2 \rightarrow f$	$2E_{1/2g} + E_{5/2g} + E_{7/2g}$	28742	348
$5e_{5/2g} \rightarrow 5e_{7/2u}$	$\pi_2 \rightarrow f$	$E_{1/2g} + E_{3/2g} + 2E_{7/2g}$	31276	320
$5e_{5/2g} \rightarrow 8e_{3/2u}$	$\pi_2 \rightarrow f$	$3E_{3/2g} + E_{7/2g}$	31291	320
$5e_{5/2g} \rightarrow 10e_{1/2u}$	$\pi_2 \rightarrow f$	$2E_{1/2g} + E_{5/2g} + E_{7/2g}$	32328	309
$5e_{5/2g} \rightarrow 9e_{3/2u}$	$\pi_2 \rightarrow f$	$3E_{3/2g} + E_{7/2g}$	38247	261
$5e_{5/2g} \rightarrow 7e_{5/2u}$	$\pi_2 \rightarrow f$	$E_{1/2g} + 3E_{5/2g}$	40036	250
$5e_{5/2g} \rightarrow 8e_{5/2u}$	$\pi_2 \rightarrow \pi_3$	$E_{1/2g} + 3E_{5/2g}$	47603	210
$5e_{5/2g} \rightarrow 6e_{7/2u}$	$\pi_2 \rightarrow \pi_3$	$E_{1/2g} + E_{3/2g} + 2E_{7/2g}$	49113	204
$6e_{3/2g} \rightarrow 6e_{5/2u}$	$\pi_2 \rightarrow f$	$E_{3/2g}$	29618	338
$6e_{3/2g} \rightarrow 9e_{1/2u}$	$\pi_2 \rightarrow f$	$E_{1/2g} + E_{3/2g} + 2E_{7/2g}$	29267	342
$6e_{3/2g} \rightarrow 5e_{7/2u}$	$\pi_2 \rightarrow f$	$2E_{1/2g} + E_{5/2g} + E_{7/2g}$	31813	314
$6e_{3/2g} \rightarrow 8e_{3/2u}$	$\pi_2 \rightarrow f$	$E_{1/2g} + 3E_{5/2g}$	31813	314
$6e_{3/2g} \rightarrow 10e_{1/2u}$	$\pi_2 \rightarrow f$	$E_{1/2g} + E_{3/2g} + 2E_{7/2g}$	32854	304
$6e_{3/2g} \rightarrow 9e_{3/2u}$	$\pi_2 \rightarrow f$	$E_{1/2g} + 3E_{5/2g}$	38767	258
$6e_{3/2g} \rightarrow 7e_{5/2u}$	$\pi_2 \rightarrow f$	$3E_{3/2g} + E_{7/2g}$	40559	247
$6e_{3/2g} \rightarrow 8e_{5/2u}$	$\pi_2 \rightarrow \pi_3$	$3E_{3/2g} + E_{7/2g}$	48186	208
$6e_{3/2g} \rightarrow 6e_{7/2u}$	$\pi_2 \rightarrow \pi_3$	$2E_{1/2g} + E_{5/2g} + E_{7/2g}$	49678	201

[a] Transitions are listed in the order of the spin−orbital energies.

$Pa(TMCOT)_2$ has an absorption maximum at 380 nm, with a shoulder at 490 nm.[11] Based on the bathochromic shift observed in other actinocene complexes when COT is replaced by TMCOT, Streitwieser et al. estimate that the absorption maximum in unsubstituted $Pa(COT)_2$ would occur at ca. 365 nm, which, as we pointed out earlier, is in excellent accord with our calculated wavelength of the $f\phi \rightarrow d\delta$ LF transition (368 nm).

Prior calculations on $Pa(COT)_2$ have led to different assignments of the proposed 365-nm transition. Our previous DV-Xα calculations, which assumed planar COT ligands and a Pa−X distance of 1.958 Å, concluded that the 365-nm absorption was likely due to either the $f \rightarrow \pi_3$ MLCT or the $\pi_2 \rightarrow f$ LMCT transitions, which were calculated to occur at 351 and 360 nm, respectively.[13] The SOCI calculations of Zhao and Pitzer concluded that the absorption is due to the $\pi_2 \rightarrow d\sigma$ LMCT transition, which had a calculated wavelength of 341 nm.[6,14] Unfortunately, neither the DV-Xα nor the spin−orbit CI calculations include the transition energy of the $f\phi \rightarrow d\delta$ transition that is favored in our present calculations. It is therefore not apparent whether this $f\phi \rightarrow d\delta$ transition would provide an acceptable assignment by these other methods. It is interesting to note that f−d transitions, such as the one proposed here for $Pa(COT)_2$, are also proposed to be a prominent feature in the electronic spectrum of $U(COT)_2$. Indeed, the SOCI calculations on uranocene find three $f \rightarrow d$ transitions as the major absorptions in the visible region,[8] although the experimental absorptions were initially proposed to be LMCT transitions.[43,44] The $f \rightarrow d$ transition energy in our DFT calculation for the protactinocene (27 200 cm^{-1}) is greater than the experimentally determined $f \rightarrow d$ transition energies (15 170−16 270 cm^{-1}) for uranocene. This observation is consistent with a stronger metal−ligand interaction for protactinocene than for uranocene, which owes to the greater radial extent of the Pa orbitals relative to those of U. We have observed this effect in other comparisons of Pa and U as well.[26,45]

Our calculations predict that the $\pi_2 \rightarrow d\sigma$ ($7e_{3/2u} - 8e_{1/2\ g}$) LMCT transition will be found at 430 nm, which is a considerably longer wavelength than that predicted by the SOCI calculations (341 nm). We believe that the two $\pi_2 \rightarrow d\sigma$ LMCT transitions at 430−435 nm are the likely origin for the low-energy shoulder reported to occur at 490 nm in the spectrum of $Pa(TMCOT)_2$.[11] These transitions are in the violet portion of the visible spectrum and are likely responsible for the characteristic golden-yellow color of protactinocene. By contrast, the SOCI calculations find no allowed electronic transitions in the visible region, and therefore those calculations do not readily explain the observed shoulder or the color of $Pa(COT)_2$. Interestingly, the SOCI calculations on uranocene overestimated the $\pi_2 \rightarrow d\sigma$ transition energy by a factor of 1.45.[8] If this same factor is applied to the SOCI calculations on $Pa(COT)_2$, the $\pi_2 \rightarrow d\sigma$ transition would be expected to occur in the visible region at ca. 490 nm.

There are several methodological reasons for the disagreement of the present calculations with the previous DV-Xα and SOCI calculations. In our DV-Xα calculations, we required the use of thermal spreading near the Fermi level in order to reach convergence, which made it difficult to consider all of the possible $f \rightarrow d$ LF transitions.[13] Although this procedure can be used reliably to obtain ground-state properties, the total energy and the orbital energies of the fractionally occupied orbitals are quite sensitive to the fractional occupation number

(43) Streitwieser, A., Jr.; Harmon, C. A. *Inorg. Chem.* **1973**, *12*, 1102.
(44) Dallinger, R. F.; Stein, P.; Spiro, T. G. *J. Am. Chem. Soc.* **1978**, *100*, 7865.
(45) (a) Bursten, B. E.; Rhodes, L. F.; Strittmatter, R. J. *J. Am. Chem. Soc.* **1989**, *111*, 2756. (b) Bursten, B. E.; Rhodes, L. F.; Strittmatter, R. J. *J. Less-Common Met.* **1989**, *149*, 207.

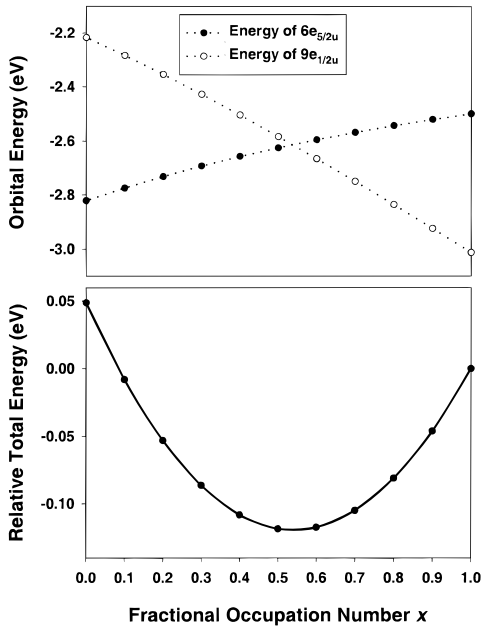

Figure 5. Variation of the energies of the $6e_{5/2u}$ and $9e_{1/2u}$ spin−orbitals (top) and of the total energy of the $(6e_{5/2u})^x(9e_{1/2u})^{1-x}$ outer electron configuration of $Pa(COT)_2$ (bottom) with the fractional occupation number x. The value $x = 1$ corresponds to the $E_{5/2u}$ ground state of the molecule.

(FON) that is determined by the thermal factor.[46] To demonstrate this sensitivity, we have performed calculations on $Pa(COT)_2$ with a fixed geometry and variable FON electron configurations $(6e_{5/2u})^x(9e_{1/2u})^{1-x}$, with x ranging from 0 to 1. The dependence of the total energy and the eigenvalues of the two fractionally occupied orbitals upon the FONs is depicted in Figure 5.[47] The dependence is exactly what one would expect in terms of the Slater−Janak relationship, $\epsilon_i = \partial E/\partial n_i$.[48] Because of the dependence of the energies on the FONs, it is most consistent to use FONs for all states or to use pure states to determine the transition energies, which is the case in our present calculations. In the case of the spin−orbit CI calculation, some other limitations appear to be in operation. First, it was not possible to optimize the geometry of $Pa(COT)_2$ with the SOCI calculations, so the geometry of $Pa(COT)_2$ was assumed to be identical to that of $U(COT)_2$. The assumed Pa−C bond distance, 2.647 Å, is significantly shorter than our PW91-optimized Pa−C distance (2.702 Å; Table 1) or the average of the M−C bond distances in $Th(COT)_2$ and $U(COT)_2$ (2.674 Å).[14] Most of the transitions in $Pa(COT)_2$ would shift to lower energy if a longer Pa−COT distance were used. Second, it was noted that neither the basis sets nor the CI expansion used in the SOCI calculations are adequate for a thorough treatment of electron correlation in actinide complexes.[6] In particular, the lack of polarization functions on the carbon atoms in the SOCI calculations may have a significant effect on the calculated transition energies involving the ligands.

Magnetic Properties. Because $Pa(COT)_2$ is an f^1 system with a single metal-localized electron, its magnetic properties might be expected to provide substantive information about the nature of the unpaired electron and of the metal−ligand interactions. The magnetic properties of f^n $M(COT)_2$ systems has been previously addressed by Warren in an elegant treatment using ligand field theory (LFT).[49] The pseudoaxial symmetry of the $M(COT)_2$ systems preserves M_J as a good quantum number. Warren treated the systems as axial under the $C_{\infty v}$* double group. For f^1 systems, he found that the ordering of the spin−orbit-coupled LFT states derived from the $^2F_{5/2}$ term follow the ordering Φ^* ($M_J = \pm 5/2$) < Π^* ($M_J = \pm 1/2$) < Δ^* ($M_J = \pm 3/2$). This conclusion is in perfect accord with our current spin−orbit DFT results for $Pa(COT)_2$, which predict a state ordering $E_{5/2u} < E_{1/2u} \ll E_{3/2u}$ (Figure 3, Table 4). As discussed earlier, the $|M_J| = 5/2$ state is the ground state as a consequence of substantial contributions of both spin−orbit and ligand-field effects; i.e., the molecule is in the "intermediate-coupling" regime.[33] The ground magnetic properties of protactinocene will be dominated by the characteristics of the $E_{5/2u}$ ground state.

In principle, the most informative magnetic data about $Pa(COT)_2$ would be obtained from its electron spin resonance (ESR) spectrum. Unfortunately, the $E_{5/2u}$ ground state is expected to be ESR-silent: when the M_J components of the $E_{5/2u}$ state are split in a magnetic field, the predicted ESR transition from $M_J = -5/2$ to $M_J = +5/2$ does not satisfy the magnetic dipole transition selection rule ($\Delta M_J = \pm 1$).[50] The first excited state, $E_{1/2u}$, is an ESR-active state that lies ca. 400 cm^{-1} above the ground state. Its thermal population at room temperature is expected to be very small but will increase as the temperature is elevated ($kT = 400$ cm^{-1} at $T = 300$ °C). In principle, therefore, $Pa(COT)_2$ could have an excited-state ESR spectrum at elevated temperatures, although it seems unlikely that this challenging experiment will be undertaken on this difficult-to-handle material. Thus, observations of the magnetic properties of $Pa(COT)_2$ are likely to be limited to studies of the magnetic moment of the compound.

The $E_{1/2u}$ and $E_{3/2u}$ excited states could be important contributors to the observed magnetic moment of $Pa(COT)_2$. By using the Van Vleck equation, which incorporates the first- and second-order Zeeman terms, one can determine the variation of magnetic moment with temperature.[51] Warren has used the Van Vleck equation to derive expressions for the parallel (z) and perpendicular (x,y) components of the magnetic moment of an axial f^1 system, with inclusion of the Φ^*, Π^*, and Δ^* states in the sum-over-states.[49] We have used Warren's formalism and the calculated PW91 state energies to determine the temperature dependence of the magnetic moment. In Figure 6, the calculated anisotropic magnetic moments μ_z (parallel) and $\mu_{x,y}$ (perpendicular), and the average magnetic moment $\langle\mu\rangle = [1/3(\mu_x^2 + \mu_y^2 + \mu_z^2)]^{1/2}$, are plotted vs T, the absolute temperature. In the calculation of the magnetic moment, the orbital reduction factor, which accounts for reduction of the angular momentum due to covalent bonding or electron delocalization from f orbitals to the ligands, is taken as $k' = 0.97$, a value found empirically by Warren to give good results for uranocene.[49] The assumption of this value of k' leads to a limiting ($T \rightarrow 0$) value of $\langle\mu\rangle = 2.06$ Bohr magnetons (μ_B).

It is seen in Figure 6 that, as the temperature increases from 0 K, $\mu_{x,y}$ is predicted to increase rapidly, whereas μ_z decreases.

(46) For discussions of the fractional occupation number approach, see: (a) Wang, S.-G.; Schwarz, W. H. E. *J. Chem. Phys.* **1996**, *105*, 4641. (b) Averill, F. W.; Painter, G. S. *Phys. Rev.* **1992**, *B46*, 2498. (c) Dunlap, B. I. In *Ab initio Methods in Quantum Chemistry II*; Lawlay, K. P., Ed.; Wiley: New York, 1987.

(47) The relative energy change with the FON (x) can be well represented by $E(x) = 0.5716x^2 - 0.6194x + 0.0482$, which gives the lowest energy for the FON configuration $(6e_{5/2u})^{0.54}(9e_{1/2u})^{0.46}$.

(48) (a) Slater, J. C.; Mann, J. B.; Wilson, T. M.; Wood, J. H. *Phys. Rev.* **1969**, *184*, 672. (b) Janak, J. F. *Phys. Rev.* **1978**, *B18*, 7165.

(49) Warren, K. D. *Inorg. Chem.* **1975**, *14*, 3095.

(50) Edelstein, N. M.; Goffart, J. In *The Chemistry of the Actinides Elements*, 2nd ed.; Katz, J. J., Seaborg, G. T., Morss, L. R., Eds.; Chapman and Hall: New York, 1986; Vol. 2, Chapter 18.

(51) Van Vleck, J. H. *The Theory of Electric and Magnetic Susceptibilities*; Oxford University Press: New York, NY, 1948.

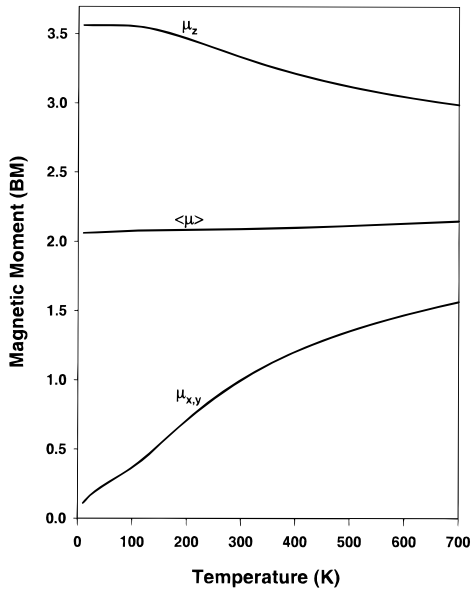

Figure 6. Calculated values of the perpendicular (μ_z) and parallel ($\mu_{x,y}$) components of the magnetic moment, and of the average magnetic moment $\langle\mu\rangle$ for $Pa(COT)_2$ as a function of temperature. The calculations are based on the derivations by Warren (ref 49).

The average magnetic moment remains nearly constant as T is changed. The calculated anisotropic room-temperature magnetic moments, μ_z and $\mu_{x,y}$ are 3.33 and 0.99 μ_B, respectively, thereby giving rise to an average magnetic moment $\langle\mu\rangle = 2.09\ \mu_B$. This calculated room-temperature magnetic moment is fairly close to the value of 1.96 μ_B that was obtained via the spin−orbit CI calculations on $Pa(COT)_2$.[14] Both values are slightly higher than the experimental room-temperature value $\langle\mu\rangle = 1.88\ \mu_B$ for the $4f^1$ sandwich anion $Ce(COT)_2^-$.[52]

Both the PW91- and SOCI-calculated values of $\langle\mu\rangle$ for $Pa(COT)_2$ are much lower than the isotropic free-ion value for an f^1 ion (2.535 μ_B), an indication of the significant Pa−ligand interactions and intermediate coupling. By contrast, the value $k' = 0.97$ might seem to indicate only a small perturbation to the ligand-field values due to covalent Pa−COT interactions. We believe that these results are not inconsistent but rather reflect the nature of the Pa−COT interaction. Our studies of organoactinide complexes indicate that the covalent metal−ligand interactions are dominated by the actinide 6d, rather than 5f, orbitals,[30,53] and we find this to be the case for $Pa(COT)_2$ as well. Thus, although there is significant covalency in the molecule, the metal-localized electron is largely unaffected by the covalent interactions, and its magnetic properties are amenable to ligand-field treatments.

Finally, we note that the calculated magnetic moments of $Pa(COT)_2$ rely considerably on the relative state energies. The calculated PW91 energy differences of the first and second excited states relative to the ground state, 393 and 2987 cm^{-1}, are in reasonable agreement with Warren's estimates from ligand-field theory, viz. 230 and 2166 cm^{-1}, respectively.[49] In addition, these energy differences of the 5f-based states in $Pa(COT)_2$ are comparable to the corresponding values in $U(COT)_2$ (466 and 2339 cm^{-1}), which were determined via Raman spectroscopy.[44,54] Therefore, we are confident that the calculated magnetic moment should provide a good estimate to the experimental value, which is thus far unknown.

Table 7. Spin-Orbital Energies (ϵ_i) and Calculated Ionization Energies (IE_i) for $Pa(COT)_2$

orbital	$-\epsilon_i$ (eV)	IE_i (eV)	assignment
$6e_{5/2u}$	2.63	5.16	fϕ
$5e_{5/2u}$	5.09	7.17	π_{2u} + fδ
$7e_{3/2u}$	5.13	7.21	π_{2u} + fδ
$5e_{5/2g}$	5.82	7.85	π_{2g} + dδ
$6e_{3/2g}$	5.90	7.93	π_{2g} + dδ
$6e_{3/2u}$	7.71	9.71	π_{1u}
$8e_{1/2u}$	7.92	9.93	π_{1u}
$5e_{3/2g}$	8.45	10.51	π_{1g}
$7e_{1/2g}$	8.47	10.53	π_{1g}
$4e_{5/2g}$	8.68	10.69	σ(C−H/C−C)
$4e_{7/2g}$	8.69	10.70	σ(C−H/C−C)
$4e_{5/2u}$	8.71	10.72	σ(C−H/C−C)
$4e_{7/2u}$	8.72	10.73	σ(C−H/C−C)
$7e_{1/2u}$	8.80	10.86	π_{0u}
$5e_{3/2u}$	9.30	11.30	σ(C−H/C−C)
$3e_{5/2u}$	9.30	11.31	σ(C−H/C−C)
$3e_{5/2g}$	9.32	11.32	σ(C−H/C−C)
$4e_{3/2g}$	9.32	11.32	σ(C−H/C−C)
$6e_{1/2g}$	9.79	11.82	π_{0g}
$3e_{7/2u}$	10.79	12.81	σ(C−H/C−C)

Ionization Energies. The experimental photoelectron spectrum of $Pa(COT)_2$ has not yet been reported. Nevertheless, we can use the present calculations to predict the ionization energies of the molecule, which may facilitate the future assignment of the photoelectron spectra. The ground-state spin-orbital energies ϵ_i and the ionization energies IE_i, calculated via Slater's transition-state method,[55] are listed in Table 7. For each orbital, $IE_i > -\epsilon_i$, consistent with the removal of 0.5e from each orbital in the transition-state method. For the ionizations listed, all but that from the $6e_{5/2u}$ HOMO are primarily ligand-based. There is an excellent linear correlation between IE_i and ϵ_i for these ligand-based ionizations:

$$IE_i = 2.106 - 0.990\epsilon_i \qquad R = 0.9999$$

This linear correlation with nearly unit slope suggests that the relaxation of the ligand-based orbitals upon removal of charge is essentially the same for all orbitals.

As expected, the first ionization corresponds to removal of the Pa-localized 5f electron. The calculated ionization energy, 5.16 eV, is considerably lower than the first ionization energy of f^2 uranocene (6.20 eV).[56] The lower IE of $Pa(COT)_2$ relative to $U(COT)_2$ reflects the more electropositive nature of Pa and is consistent with periodic trends on the 5f orbital energies as one proceeds across the actinide series. The small IE of $Pa(COT)_2$, comparable to that of a sodium atom (5.14 eV), suggests that $Pa(COT)_2$ is a highly reducing complex that will readily form an f^0 Pa(V) product. This conclusion is consistent with the extreme air sensitivity of $Pa(COT)_2$, which has made it more difficult to synthesize and study than other actinocene complexes.[10]

The next lowest IEs of $Pa(COT)_2$ correspond to ionization of the π_2 orbitals of the COT ligands. Ionization from the π_{2g} orbitals, which are stabilized by interaction with the Pa 6d orbitals, is predicted to require ca. 0.7 eV greater energy than ionization from the π_{2u} orbitals, which interact with the Pa 5f orbitals. This observation is consistent with the primary role of the Pa 6d rather than 5f orbitals in the Pa−COT bonding, as has been found in both experimental[56] and theoretical[7,8] studies

(52) Hodgson, K. O.; Mares, F.; Starks, D. F.; Streitwieser, A. *J. Am. Chem. Soc.* **1973**, *95*, 8650.
(53) Burns, C. J.; Bursten, B. E. *Comments Inorg. Chem.* **1989**, *9*, 61.
(54) Amberger, H. *J. Less-Common Met.* **1983**, *93*, 235.
(55) Slater, J. C. *Quantum Theory for Molecules and Solids. The Self-Consistent Field for Molecules and Solids*; McGraw-Hill: New York, 1974; Vol. 4.
(56) Brennan, J. G.; Green, J. C.; Redfern, C. M. *J. Am. Chem. Soc.* **1989**, *111*, 2373.

Table 8. LDA and PW91 Calculated Vibrational Frequencies (cm^{-1}) and Absolute Intensities (km/mol) for the Allowed Infrared Modes of $Pa(COT)_2$[a]

mode	calcd LDA	calcd PW91	expt[b]	assignment[c]
A_{2u}	238 (31.0)	240 (31.8)	*245* (s)	X−Pa−X stretch
	695 (357)	684 (296)	695 (vs)	X−C−H bend
	756 (3.8)	772 (76.3)	745 (s)	C−C stretch
	3046 (33.9)	3065 (26.0)	*3005* (m)	C−H stretch
E_{1u}	46i (−9.0)	33 (11.6)	135	X-Pa-X bend
	230 (0.0)	221 (0.6)		Pa−COT tilt
	747 (31.6)	762 (36.8)	775 (m)	C−C stretch
	914 (62.8)	896 (81.4)	895 (s)	X−C−H bend
	1404 (3.2)	1438 (0.0)	1310 (m)	C−C−H bend
	3045 (8.0)	3063 (17.8)	*2920* (m)	C−H stretch

[a] The calculated absolute intensities in km/mol are given in parentheses after the calculated frequencies in cm^{-1}. [b] Experimental data are from ref 10b. Experimental values in italics are estimates based on the experimental values for thorocene and uranocene.[59] The experimental intensities are given in parentheses as very strong (vs), strong (s), and medium (m). [c] Assignments shown are the principal components of the calculated normal mode eigenvectors. X denotes the centroid of the COT ligand. X−C−H bends are out-of-plane bending modes, whereas the C−C−H bend is an in-plane bending mode.

of uranocene and in our DV-Xα studies of protactinocene.[13] The mean calculated π_{2u} and π_{2g} IEs in $Pa(COT)_2$ (7.2 and 7.9 eV, respectively) are very comparable to the experimentally assigned π_{2u} and π_{2g} ionizations in $Th(COT)_2$ (6.79 and 7.91 eV)[57] and in $U(COT)_2$ (6.90 and 7.85 eV).[56,57] The remaining IEs in Table 7 correspond to primarily ligand-based ionizations from the π_1, π_0, and C−C and C−H σ orbitals of $Pa(COT)_2$.

The filled ligand-based π_{1g}, π_{1u}, π_{2g}, and π_{2u} orbitals are all subject to spin−orbit splitting under the D_{8h}* double group. The spin−orbit splittings of the COT π_{1g} ($7e_{1/2g} + 5e_{3/2g}$), π_{2g} ($6e_{3/2g} + 5e_{5/2g}$), and π_{2u} ($7e_{3/2u} + 5e_{5/2u}$) are all rather small, i.e., 0.02, 0.08, and 0.04 eV, respectively. Interestingly, the π_{1u} ($8e_{1/2u} + 6e_{3/2u}$) orbitals undergo significant spin−orbit splitting of 0.22 eV, based on the calculated IEs. This larger spin−orbit splitting is attributed to 6p contributions to these orbitals; because the 6p orbitals undergo much larger spin−orbit coupling than do the 6d or 5f orbitals, a marked splitting results even though the contributions of the 6pπ orbitals to the π_{1u}-based spin−orbitals are only about 2%. This phenomenon has been observed previously in the photoelectron spectra of OsO_4.[58]

Infrared-Active Vibrations. Among the few spectroscopic investigations of $Pa(COT)_2$ that have been carried out is an infrared (IR) spectroscopic study by Goffart, Duyckaerts, and co-workers,[10b,59] which showed that its spectrum was similar to those of other actinocenes. Thus far, only a tentative vibrational assignment of thorocene and uranocene, based on qualitative group theory analysis, is available. We will therefore conclude our discussion with a brief comparison of our calculated IR frequencies and intensities of $Pa(COT)_2$ with the available experimental data. These calculations have been carried out by calculating numerical second derivatives at the minimum-energy geometries with both the LDA and PW91 functionals, including scalar relativistic corrections.

The protactinocene molecule has 93 fundamental normal modes. Under D_{8h} symmetry, only the four A_{2u} and six E_{1u} modes are IR-active.[60] Table 8 lists the calculated LDA and PW91 IR frequencies and absorption intensities as well as the available experimental frequencies. The important metal−ligand vibrational modes can be obtained by assuming a linear triatomic model, in which each COT ligand is considered as a single center. The three vibrational modes under this model are (1) the symmetric ring−metal−ring stretching mode (A_{1g}, Raman active), (2) the antisymmetric ring−metal−ring stretching mode (A_{2u}), and (3) the doubly degenerate ring−metal−ring bending mode (E_{1u}). These three modes are the lowest-frequency Raman and IR vibrations of protactinocene.

Based on the experimental IR spectra of thorocene and uranocene,[59] the antisymmetric ring−metal−ring stretching mode in $Pa(COT)_2$ is expected to have a strong IR absorption that is estimated to occur at 245 cm^{-1}. Both the LDA- and PW91-calculated frequencies (238 and 240 cm^{-1}, respectively) are in excellent accord with this estimate. The antisymmetric ring−metal−ring bending mode of $Pa(COT)_2$ is expected to occur even lower in energy; based on the frequencies in thorocene and uranocene, we estimate that it should be observed at ca. 135 cm^{-1}. The potential energy surface for this mode is so flat that the calculated frequency of this mode becomes imaginary in the LDA calculation. The higher-level PW91 calculation leads to a calculated frequency of 33 cm^{-1} for this mode.[61] The most intense IR absorption of protactinocene occurs at 695 cm^{-1}, a band that was initially assigned to the E_{1u} antisymmetric ring−metal tilting mode.[59] Our calculations suggest that this assignment is incorrect; we find an intense A_{2u} vibration, corresponding to an out-of-plane C−H bending mode, with a PW91-calculated frequency of 684 cm^{-1} as the best assignment of this band. This vibrational frequency is essentially constant across the $M(COT)_2$ series, with M = Th, Pa, U, and Np exhibiting experimental frequencies of 695, 695, 698, and 690 cm^{-1}, respectively.[10b] The invariance of this band to the metal center corroborates its assignment as an essentially purely ligand-based vibration. All of the higher-frequency vibrations are also assigned to ligand-based (C−C stretching, C−C−H bending, C−H stretching) vibrations. Overall, the calculated vibrational frequencies and intensities at the PW91 level provide a good correlation with the experimental spectra. The LDA calculations provide reasonably good results except for the problems with very low frequency vibrations.

Concluding Comments

Because of the scarcity and radioactivity of protactinium, protactinocene and other Pa-containing complexes are very difficult to study experimentally. Thus, reliable theoretical studies of such molecules can provide important guidance in the interpretation of hard-to-obtain experimental data. The gradient-corrected density functional calculations on $Pa(COT)_2$, with spin−orbit effects included as appropriate, provide excellent agreement with the limited available experimental data on the complex. Among ground-state properties of the molecule, the calculated vibrational frequencies are in good agreement with the experiment, and it seems likely that the predicted geometry will ultimately be tested via crystallographic studies. The calculated ionization energies can serve as a guide in future experimental assignment of the photoelectron spectra of this compound. With respect to excited-state properties, we note that DFT is generally considered to be most valid for the ground

(57) Clark, J. P.; Green, J. C. *J. Chem. Soc., Dalton Trans.* **1977**, 505.
(58) Bursten, B. E.; Green, J. C.; Kaltsoyannis, N. *Inorg. Chem.* **1994**, *33*, 2315.
(59) Hocks, L.; Goffart, J.; Duyckaerts, G.; Teyssie, P. *Spectrochim. Acta* **1974**, *30A*, 907.
(60) Cotton, F. A. *Chemical Applications of Group Theory*, 3rd ed.; Wiley: New York, 1990.

(61) Because of the flatness of the potential surfaces for these low-energy vibrations, we have increased the numerical integration accuracy of our calculations relative to the state energy calculations. In the ADF method, that corresponded to an increase in the INTEGRATION parameter from 6.0 to 8.0. At the PW91 level, this increased integration accuracy assured that none of the frequencies were imaginary.

states of molecules. Nevertheless, the present calculations indicate that gradient-corrected DFT methods with the explicit inclusion of spin−orbit coupling can be used to predict the excited state properties of actinide complexes (at least those with formally only one valence 5f electron).

Our future efforts in this area will address a much harder problem, namely the excited states of actinide complexes with two or more 5f electrons, such as uranocene. The multiplet structure of such molecules in the presence of significant spin−orbit coupling promises to be a great challenge. Nevertheless, given the success of DFT methods in dealing with the multiplet problem in transition metal compounds,[62] these extensions of gradient-corrected DFT methods to many-f-electron systems should prove to be very interesting and promising.

(62) Daul, C. A.; Doclo, K.; Stueckl, C. In *Recent Advances in Density Functional Methods (Part II)*; Chong, D. P., Ed.; World Scientific Publishing Co.: River Edge, NJ, 1997.

Acknowledgment. We gratefully acknowledge financial support for this research from the Division of Chemical Sciences, U.S. Department of Energy (Grant DE-FG02-86ER13529), and from Los Alamos National Laboratory. We are also grateful to the Ohio Supercomputer Center for a grant of computer time.

JA9821145